Novel Dynamic Inversion Architecture Design for Quadrocopter Control

Jian Wang, Thomas Bierling, Leonhard Höcht, Florian Holzapfel,
Sebastian Klose, and Alois Knoll

Abstract. This paper presents a novel controller architecture for a quadrocopter. A two-loop controller using dynamic inversion is designed that allows direct commands for position and heading angle. The inner loop controls the body-fixed angular rates. And the outer loop achieves the position control. With this structure, the position dynamic equation appears in an elegant form. The derived controller is capable of decoupling the strongly coupled dynamics of the quadrocopter, maximizing the transmission bandwidth of the position control, as well as eliminating the singularity caused by the attitude control (i.e. pitch angle at 90 degree). Pseudo-control hedging is applied in the position loop to account for limitations, saturations, actuator dynamics and delay in the inner loop. The effectiveness of the designed controller is demonstrated by an implementation on a quadrocopter equipped with an ARM7 onboard processor.

Nomenclature

B	Body-fixed frame
W	World frame, deduced from NED frame with user-defined x-axis
M_{BW}, M_{WB}	Transformation matrices between B frame and W frame
L, M, N	The moments around x, y and z axis of B frame, respectively
p, q, r	Angular rates around x, y and z axis of B frame, respectively
$(\bar{r})_W$	Position vector denoted in W frame
$(\bar{V})_W^W$	Velocity vector defined w.r.t. W frame denoted in W frame

Jian Wang · Thomas Bierling · Leonhard Höcht · Florian Holzapfel
Institute of Flight System Dynamics, TU München, Germany, 85748

Sebastian Klose · Alois Knoll
Institute of Robotics and Embedded Systems, TU München, Germany, 85748

$\left(\bar{a}\right)_W^{WW}$	Acceleration vector defined w.r.t. W frame denoted in W frame
$\left(\dot{\bar{a}}\right)_W^{WWW}$	Acceleration vector differentiated w.r.t. W frame
$\bar{\gamma}_W$	Gravitational vector in W frame
$\bar{f}_B$	Specific force vector in B frame, accelerometer output.
T	Total thrust of the quadrocopter

1 Introduction

Recent technological progress in low-cost MEMS-based sensors, actuators and energy storage devices enables the development of miniature vertical take-off and landing (VTOL) systems. The quadrocopter is one of the most preferred types for many civil applications as well as research platforms. There are many advantages, like easy construction and steering principle, VTOL and hovering ability. However, because of the nonlinear dynamic behavior, the control and guidance of these vehicles is a subject of research, especially in applications such as search and rescue, surveillance, inspection, and so on. For these applications, high stability, high precision hovering ability, high bandwidth, and high maneuverability are important.

Previous effort on nonlinear dynamic inversion control for Micro Aerial Vehicles (MAV) include three-loop design corresponding to inversion of rotational, attitude and path dynamics in separated cascaded loops[1]. A more common controller architecture is two-loop design [2]-[4], where the outer loop is the position control and the inner loop provides attitude control, as illustrated in Fig. 1. Both control loops have relative degree 2 dynamics. But they have a limited bandwidth and a singularity occurs at a Pitch angle of 90° when Euler angles are used [2].
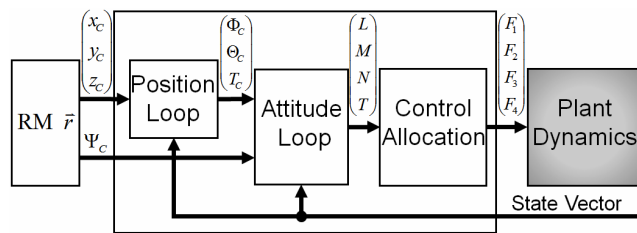

Fig. 1 Conventional two loops control architecture

The focus of this work is on the design of a baseline controller using the nonlinear dynamic inversion method. The system is capable to utilize the high bandwidth of the system and full actuator range without instability caused by actuator saturation. It can thus be used as a solid basis to apply augmented control philosophies, e.g. adaptive control. In addition to the functional requirement, the control

algorithm has to be implemented in the embedded hardware and has to fulfill real-time requirements while limited memory and onboard processing capacity have to be considered. Detailed derivation of the control law design is illustrated, followed by the flight test data to verify the design. For the flight test, vision sensors are used to aid the inertial sensors embedded onboard. Details about the visual processing and the experimental setup can be found in [2]. Specific sensor data fusion, trajectory planning and protection mechanisms for takeoff and landing are integrated for the flight test.

2   Dynamics of the Quadrocopter

One well-known inherent quadrocopter characteristics is the strong coupling in pitch-yaw-roll. A tradeoff often has to be made between maximization of the system bandwidth and dynamic decoupling. Both problems can be confronted in an elegant way if we look at the reaction of the quadrocopter on changes of rotational rates of the propellers as follows:
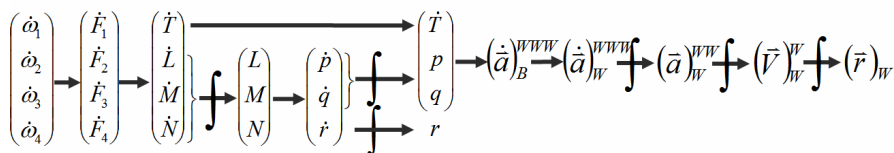
$$\begin{pmatrix} \dot{\omega}_1 \\ \dot{\omega}_2 \\ \dot{\omega}_3 \\ \dot{\omega}_4 \end{pmatrix} \rightarrow \begin{pmatrix} \dot{F}_1 \\ \dot{F}_2 \\ \dot{F}_3 \\ \dot{F}_4 \end{pmatrix} \rightarrow \begin{pmatrix} \dot{T} \\ \dot{L} \\ \dot{M} \\ \dot{N} \end{pmatrix} \Bigg\} \begin{pmatrix} L \\ M \\ N \end{pmatrix} \rightarrow \begin{pmatrix} \dot{p} \\ \dot{q} \\ \dot{r} \end{pmatrix} \Bigg\} \begin{pmatrix} \dot{T} \\ p \\ q \\ r \end{pmatrix} \rightarrow \left(\dot{\bar{a}}\right)_B^{WWW} \rightarrow \left(\dot{\bar{a}}\right)_W^{WWWW} \rightarrow \left(\bar{a}\right)_W^{WW} \rightarrow \left(\bar{V}\right)_W^{W} \rightarrow \left(\bar{r}\right)_W$$

Fig. 2 Signal flow diagram of the quadrocopter dynamics

As shown in Fig. 2, a change in the rotational rate of each propeller results in changes in the thrust of each motor, which gives the change of total thrust and the body-fixed rotational moments. These moments result in body fixed angular accelerations, and consequently the angular rates. Then the angular rates p, q and the change in the total thrust yield a change in the acceleration with respect to the world frame. The change in acceleration in the end results in change of the position by three integrations.

The resulting change in acceleration in the body frame consists of 2 integrations in the x_B-y_B-plane, whereas in the direction of the z_B-axis acceleration directly results from the change in thrust. Different axes of the position dynamics are coupled with different dynamic orders. It is difficult to perform exact input-output feedback from position to the motor thrusts. A dynamic inversion of the position dynamics with relative degree 3 however is possible.

As can be seen in the signal flow diagram in Fig. 2, attitude angles are not included, but only implicitly appear in the transformation matrix. The inputs for the translation dynamics extend to change of acceleration, i.e. angular rate and change of thrust. In other words, position can be controlled by a more direct input, which

certainly increases the bandwidth of the position control. Thus the dynamic inversion of the position dynamics with relative degree 3 is dynamically correct, and the complexity of the dynamic inversion is manageable with potential increase in the bandwidth.

For the yaw control, there will be coupling from position dynamics if the azimuth angle is used as the control variable. From Fig. 2, the yaw dynamics, however, is not inherently coupled with the translational dynamics. Hence a simple way to solve the problem is to control the yaw rate directly, but with an integral part in the error controller. Considering the drift rate of the gyro (200° /hour), the heading can be well controlled, without coupling with the translational dynamics.

In summary, the new control structure is an outer loop position control of relative degree 3 and an inner loop rate control of relative degree 1. In the next chapter, the mathematic derivation for the dynamic inversion is explained in detail.

3 Dynamic Inversion

Dynamic inversion is an approach where feedback linearization is applied to the outputs of interests. It addresses the problem of controller design by transforming a nonlinear system to a linear one by feedback. The transformed plant, as an equivalent linear system, may be analyzed by all means of linear system and control theory. [5] [6]

3.1 Inner Loop – Rotational Dynamics

The inner loop commands angular rates and generates moment commands $\left(\bar{M}_{des}^{G}\right)_B$ for the control allocation. The rotational dynamics are well known. By neglecting the aerodynamic moment in the moment dynamics, the desired moment command is directly obtained by,

$$\left(\bar{M}_{des}^{G}\right)_B = I_{BB}^{G} \cdot \left(\dot{\bar{\omega}}^{OB}\right)_B + \left(\bar{\omega}^{OB}\right)_B \times I_{BB}^{G} \cdot \left(\bar{\omega}^{OB}\right)_B \tag{1}$$

3.2 Outer Loop-Translation Dynamics

The command to the outer loop is the desired position in the W-frame, from which it generates an angular rate command that is issued to the inner loop. Starting from Newton's 2nd law, we can derive the translational equation of motion by assuming that the W-frame can be used as inertial frame,

$$m \cdot (\bar{a})_W^{WW} = \left(\bar{F}^{G}\right)_W + \left(\bar{F}_{Grav}^{G}\right)_W + \left(\bar{F}_{Aero}^{G}\right)_W \tag{2}$$

For a quadrocopter the aerodynamic lift and side force are negligible and the aerodynamic drag coefficient can be assumed to be constant for simplicity. With these assumptions, equation (2) can be rewritten as,

$$(\bar{a})_W^{WW} = M_{WB}\bar{f}_B + \bar{\gamma}_W - d_W = M_{WB}\begin{bmatrix} 0 \\ 0 \\ -T/m \end{bmatrix} + \begin{bmatrix} 0 \\ 0 \\ g \end{bmatrix} - d_W \tag{3}$$

Where $d_W = \dfrac{1}{2m}C_D\rho S\left\|(\bar{V})_W^W\right\| \cdot (\bar{V})_W^W$. As the inner loop inputs have not appeared, Eqn. (3) is differentiated

$$(\dot{\bar{a}})_W^{WWW} = \dot{M}_{WB}\bar{f}_B + M_{WB}\dot{\bar{f}}_B - \dot{d}_W \tag{4}$$

Where $\dot{d}_W = \dfrac{1}{2m}C_D\rho S\left[\dfrac{\left[(\bar{V})_W^W\right]^T \cdot (\bar{a})_W^{WW}}{\left\|(\bar{V})_W^W\right\|} \cdot (\bar{V})_W^W + \left\|(\bar{V})_W^W\right\| \cdot (\bar{a})_W^{WW}\right]$ and the Euler differentiation rule can be used,

$$\dot{M}_{WB} = M_{WB} \cdot \Omega^{WB}, \text{ and } \Omega^{WB} = skew\left(\bar{\omega}^{WB}\right)_B \tag{5}$$

Hence Eqn. (4) becomes

$$(\dot{\bar{a}})_W^{WWW} = M_{WB}\begin{bmatrix} -T/m \cdot q \\ T/m \cdot p \\ -\dot{T}/m \end{bmatrix} - \dot{d}_W \tag{6}$$

Now the angular rates explicitly appear in the equation. The first order time derivative of acceleration is the third order time derivative of the position. So the relative degree for position dynamics is three as expected. By the zeros in the first two rows of the specific force vector $\bar{f}_B$, the yaw rate is algebraically cancelled out.

The coupled dynamics can be inverted analytically using Eqn. (6). Here we can replace the 3rd order time derivative of the position with the pseudo control $v = (\dot{\bar{a}})_W^{WWW}$

$$\begin{bmatrix} q \\ p \\ \dot{T} \end{bmatrix} = m\begin{bmatrix} -1/T & 0 & 0 \\ 0 & 1/T & 0 \\ 0 & 0 & -1 \end{bmatrix} M_{BW} \cdot \left(v + \dot{d}_W\right) \tag{7}$$

A distinguished advantage here is that, the attitude of the quadrocopter (be it Euler angle or Quaternion) is not a controlled state. This leads to the dynamic inversion equation of such a simple form and does not result in singularities usually caused by the attitude. The only singularity in the above inversion is thrust = 0, which can be easily remedied in the implementation. Theoretically this control law is capable of flying loops, inverted fast descending, etc.

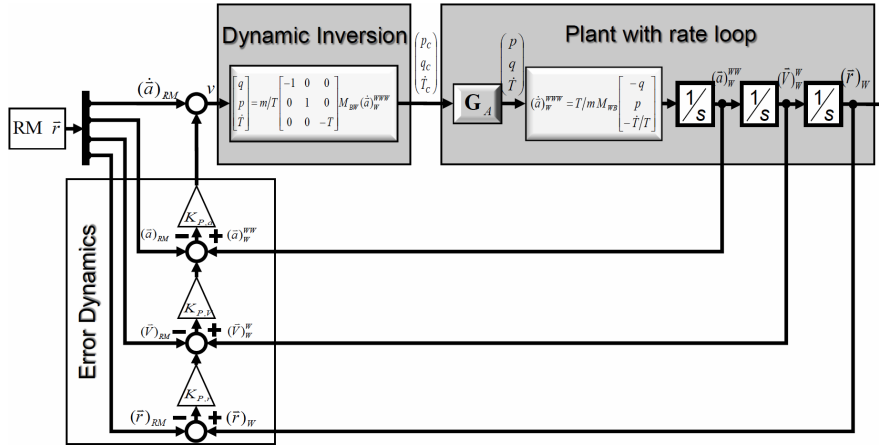The overview of the outer loop design is illustrated in Fig. 3,

Fig. 3 Overview of the position controller

4 Implementation of the Two-Loop Design

The controller was implemented on an ARM 7 processor, using the Simulink Quadrocopter Framework [7]. Critical parts of the control system like the inner loop, control allocation and data fusion are running with an update rate of 1 kHz [2]. With such a fast update rate, control deviation due to the dynamic inversion error can be quickly compensated.

4.1 Quadrocopter Specifics

The structure of the nonlinear dynamics of the quadrocopter is well known but some of the parameters have to be measured, which are listed in Table 1 below.

  'l' is the arm length between the motor and center of mass. k_n and k_m are motor specific parameters and M_{prop} is the yaw moment generated by the propellers, $F_{prop} = k_n \cdot n^2$, $M_{prop} = k_m \cdot F_{prop}$ [8].

Table 1 Quadrocopter Specific Parameters

Mass (kg)	0.68	$I_{xx} (= I_{yy})$	0.007	$k_n (10^{-8}\,\text{N/rpm}^2)$	5.7
l(m)	0.17	I_{zz}	0.012	k_m(m)	0.016

4.2 Actuator Saturations and Sensor Limitation

The thrust per motor is in the range of 0.05 N to 3.5 N [8]. Thus the moment generated can be calculated easily. To control the moment while keeping the total

thrust unchanged, the thrust difference per motor have to be symmetric. Thus the control range of each motor around the hover point is about ±1.6N. The maximum moment and angular acceleration for each axis are calculated and listed in Table 2.

Table 2 Actuator Saturations

$M_x(=M_y)$(Nm)	±0.544	M_z(Nm)	±0.102
$\dot{p}(=\dot{q})$(rad/s^2)	±77.7	$\dot{r}$(rad/s^2)	±8.5

For sensors, the Gyro is limited to a maximum value of 300°/s for the angular rates. The accelerometer measures accelerations with a full-scale range of ±1.5g, while the operation range is ±3g. The visual tracking system [2] is using a model based tracking algorithm with a stereo camera setup consisting of two standard webcams. The tracking system has an update rate of 25Hz and a speed limitation of about 1m /s due to motion blur in the images. The accuracy level varies with the lighting situation, the quadrocopter attitude and speed.

4.3 Reference Model

The reference model, or command filter is designed to generate smooth trajectories which is physically possible for the vehicle to fly. System relative degree, actuator dynamics, as well as actuator saturations and sensor limitations are taken into account.

4.3.1 Inner Loop Reference Model

The moment dynamics have angular rates as outputs and moments as inputs (see Eqn. 1). These dynamics have only relative degree one. However, in order to explicitly account for motor dynamics, a second order reference model is used instead of a first order reference model. Hence the second order time derivative can be limited. The additional pole can be placed with a small time constant: 0.002s.

In the experiments [8], the time constants of the propulsion dynamics are found to be 1/80s for increasing thrust and 1/40s for decreasing thrust. A simulation model has been constructed to assess and maximize the bandwidth of the inner loop, which determines the time constant of the slower pole.

4.3.2 Outer Loop Reference Model

For the outer loop, there are three integrations between the inputs (angular rates and the change of Thrust) and outputs (position in W frame). Hence a third order reference model is used. The time scale separation has to be considered in the outer loop. Compared with the attitude control inner loop shown in Fig. 1, the designed rate control inner loop allows smaller time scale separation, i.e. higher bandwidth, for the position control outer loop. In flight test, the increase in the bandwidth is not so distinct, as the major limitation comes from the vision system

[2]. Nevertheless, the optimal Eigenvalues of the outer loop designed in [2], where attitude control was used as inner loop, were at '-4', while the optimal Eigenvalues of the outer loop are now assigned at '-5'. The differential equation of the 3rd order reference model is shown below, with ω_0=5.

$$\dddot{y}_R + 3\omega_0 \ddot{y}_R + 3\omega_0^2 \dot{y}_R + \omega_0^3 \cdot y_R = \omega_0^3 \cdot y_c \qquad (8)$$

4.4 Error Controller

With exact dynamic inversion the outputs would exactly follow the reference trajectories. Due to the model uncertainties such as parameter error and sensor error, the 3rd order time derivatives of the vehicle position differ from the dedicated pseudo control. The effect is propagated through the integration and leads to a difference between plant outputs and reference signals. The error controller uses feedback of the state errors, augmented by an integral error control to achieve steady state accuracy. [9].

For the outer loop, the error dynamics is expressed by Eqn. (9), where $e = y_{ref} - y$

$$v = \dddot{y}_{ref} + K_{d2} \cdot \ddot{e} + K_{d2} \cdot K_d \cdot \dot{e} + K_{d2} \cdot K_d \cdot K_p \cdot e + K_i \cdot \int e \cdot dt \qquad (9)$$

The error dynamics can be adjusted by the coefficients K, to follow the reference dynamics. The integral gain can be determined by pole placement and a small value is chosen to ensure steady state accuracy while not affecting the performance.

$$K_{d2} = 3\omega_0, \ K_d = \omega_0, \ K_p = \frac{\omega_0}{3} \qquad (10)$$

4.5 Control Allocation

For the quadrocopter, the relationship between the forces & moments and the propulsion controls are invertible. The desired force and moment commands are denoted with the subscript 'des'.

$$\begin{pmatrix} L_{des} \\ M_{des} \\ N_{des} \\ T \end{pmatrix} = \begin{bmatrix} 0 & -l & 0 & l \\ l & 0 & -l & 0 \\ k_m & -k_m & k_m & -k_m \\ 1 & 1 & 1 & 1 \end{bmatrix} \cdot \begin{pmatrix} F_1 \\ F_2 \\ F_3 \\ F_4 \end{pmatrix} \qquad (11)$$

4.6 Pseudo Control Hedging

Pseudo Control Hedging (PCH) is implemented to 'hide' the actuator dynamics from the error dynamics [10]. The expected reaction of the plant $\hat{v}$ is calculated

using Eqn. (6), in which the angular rates are taken from the Gyro measurements, the thrust and change of thrust are estimated by means of the modeled actuator dynamics $\hat{G}_A(\dot{T}, T)$, as they are not measureable.

$$\hat{v} = \hat{F}\left(p, q, \hat{G}_A(\dot{T}, T)\right) \tag{12}$$

Then the hedging signal or the expected reaction deficit can be calculated by $v_h = v - \hat{v}$.

The dynamics of the reference model is decelerated by the expected reaction deficit. Another function of PCH is to prevent the integrator to wind up in the error dynamics [10]. This can be demonstrated in experiment (Fig. 4(e)) by introducing an external displacement disturbance to the hovering quadrocopter.

4.7 Sensor Data Fusion

To achieve high bandwidth control, fast data fusion is important. There is not enough computation power on the ARM 7 processor for a standard full state Kalman Filter with fast update rate. Instead, a model based Kalman state estimator is implemented to fuse the sensor data. The dynamic nature and system orders are taken into account in the filter, i.e. third order dynamics in x- and y-axes and second order dynamic in z- axis. Hence the inputs are time derivatives of the accelerations for x- and y- axes calculated using Eqn. (6) and acceleration in z axis obtained from the accelerometer. In total there are 9 states: 3 axes position, 3 axes velocities, and accelerations in x- and y- axes and acceleration bias in z axis. Acceleration bias in x- and y- axes is unobservable as an AHRS (Attitude Heading Reference System) filter is used to estimate the quaternions. There are five measurements, three positions obtained from the visual tracking system and two accelerations in x-y axes from the accelerometer. The constant Kalman gain matrix (9×5) is calculated as the optimal Kalman gain for the system offline, given the process noise and measurement covariance [11].

The vision system uses two standard web cameras to track the quadrocopter, based on edge matching algorithms [2]. The measured output is the position vector in the World frame at approximately 25Hz with variable accuracy (2cm -10cm). The latency of the vision system is about 100ms and it is taken into account by adjusting the position measurement with velocity compensation.

The most important advantage of the state estimator is that it is running onboard with an update rate of 1 kHz. Therefore, disturbances detected by the IMU can be compensated within milliseconds. The filter also significantly reduces the noise originated from the thermal accelerometer measurements [13]. Overall, the filter shows very fast reaction and little noise.

5 Experimental Results

In order to show the performance of the new controller, different trajectories like circle, infinity sign, and step commands have been tested with data recorded
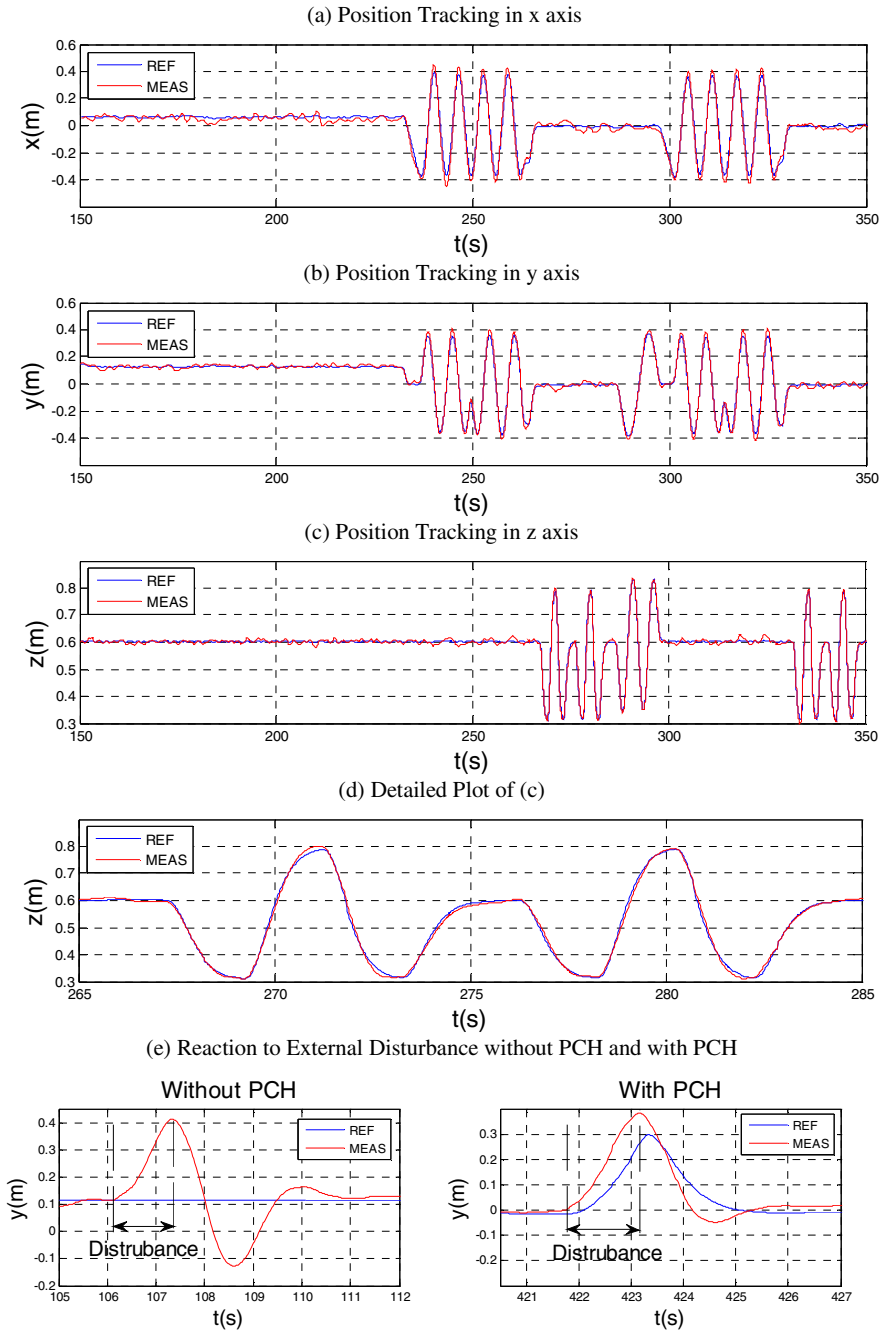
Fig. 4 Experimental Results of Trajectory Flights

online. To show the accuracy of the system, the reference commands and the vision sensor measurement are plotted. It can be seen in Fig. 4 (a-d) that the position tracking is nearly perfect: the control errors are relatively small (within 5cm) esp. in the z axis. The inter-axis coupling is negligible. The robustness and performance of the system has been demonstrated in two international trade fairs, 'Embedded World 2010' and 'ELECTRONICA 2010' held in Germany, where it was flying approximately 8 hours every day during the fairs.

The effect of PCH can be seen in (e) and (f) of Fig. 4. Big overshot caused by the integrator wind-up can be compensated by the hedging signals that change the reference signals in case of actuator saturations.

6 Conclusion

With the current position controller and the vision sensor, the quadrocopter is able to fly with good accuracy and a comparatively higher bandwidth. Based on the available structure, new control theory and application, like adaptive control and advanced data fusion are of interest to the author and to be developed.

Acknowledgments

References

1. Holzapfel, F., Sachs, G.: Dynamic Inversion Based Control Concept with Application to an Unmanned Aerial Vehicle. In: AIAA Guidance, Navigation and Control Conference and Exhibit: AIAA-2004-4907 (2004)
2. Klose, S., Wang, J., et al.: Markerless Vision Assisted Flight Control of a Quadrocopter. In: IEEE 2010 RSJ International Conference on Intelligent Robots and Systems (2010)
3. Voos, H.: Nonlinear Control of a Quadrotor Micro-UAV using Feedback-Linearization. In: Proc. of IEEE International Conference on Mechatronics (2009)
4. Bouabdallah, S., Siegwart, R.: Backstepping and Sliding-mode Techniques Applied to an Indoor Micro Quadrotor. In: Proc. of the IEEE International Conference on Robotics and Automation (2005)
5. Marquez, H.: Feedback linearization. In: Nonlinear Control Systems – Analysis and Design. Wiley, Canada (2003)
6. Khalil, H.: Feedback linearization. In: Nonlinear Systems, 3rd edn. Prentice Hall, Englewood Cliffs (2002)
7. Achtelik, M.: Simulink Quadrocopter Framework. Semesterarbeit, Technische Universität München (2009)
8. Achtelik, M.: Nonlinear and Adaptive Control of a Quadcopter, Diplomarbeit, Technische Universität München (2010)

9. Holzapfel, F.: Nichtlineare adaptive Regelung eines unbemannten Fluggerätes. PhD thesis, Technische Universität München (2004)

10. Johnson, E.: Limited Authority Adaptive Flight Control. PhD thesis, Georgia Institute of Technology (2000)

11. Franklin, F., Powell, D., et al.: Digital Control of Dynamic System, 2nd edn. Addison-Wesley, Reading (1990)

12. Ascending technologies GmbH, Hummingbird Autopilot (2010),
    `http://www.asctec.de` (accessed July 27, 2010)

13. MEMSIC, Inc., Thermal Accelerometer (August 27, 2010),
    `http://www.memsic.com`